IGNITION AND COMBUSTION CHARACTERISTICS OF METALLIZED PROPELLANTS

Semi-Annual Report
(January 1990-June 1990)

Prepared by

S. R. Turns, D. C. Mueller, and M. J. Scott

Grant No. NAG 3-1044
Bryan Palaszewski
NASA Technical Officer

July 1990

IGNITION AND COMBUSTION CHARACTERISTICS OF METALLIZED PROPELLANTS

Semi-Annual Report

(January 1990-June 1990)

Prepared by

S. R. Turns, D. C. Mueller, and M. J. Scott

Department of Mechanical Engineering
and the
Center for Space Propulsion Engineering
The Pennsylvania State University
University Park, PA 16802

for

NASA Lewis Research Center

Grant No. NAG 3-1044

Bryan Palaszewski
NASA Technical Officer

July 1990

SUMMARY

Shakedown and calibration of the experimental apparatus designed to study secondary atomization and ignition characteristics of aluminum slurry propellants was begun and nears completion. The burner was tested over an array of equivalence ratios and oxygen mass fractions to determine the permissible range of operating conditions. A burner flow control system has been designed and fabricated which permits independent control of flame stoichiometry and oxidant O_2 concentrations. The Sun slurry formulation was selected as the base for initial testing. Laser beam waists at the focal volume of the single-particle sizing system were determined to be 396 μm for the Ar-ion and 81 μm for the He-Ne laser. Size calibrations using pinholes were completed and compared to Mie theory for light scattering from particles. A vibrating orifice droplet generator was used to test the single-particle sizing system dynamically by producing a water droplet laden gas flow. The data acquisition and analysis programming has been completed and testing is in progress. From initial results, the particle sizing, atomization and ignition detection systems appear to be performing as expected. Plans for the next six months include parametric studies of the baseline slurry and preliminary formulation of a disruptive ignition model.

TABLE OF CONTENTS

PARTICLE SIZING AND VELOCITY DIAGNOSTICS

OPTICAL SYSTEM

Calibration

The procedures and hardware used to determine particle size and particle velocity are as described in the January 1990 Semi-Annual Report with the exception of the Ar-ion laser wavelength. Due to an unstable operating condition of the Ar-ion laser at the 488 nm wavelength, the wavelength of the primary beam was changed to 514.5 nm, which resulted in stable operation of the Ar-ion laser. The filter on the forward scatter receiving channel photomultiplier tube was replaced with a 514.5 nm filter.

The first task in calibration of the particle sizing set-up is the concentric alignment of the two laser beams and the determination of the beam waists. This is accomplished by radially traversing each beam separately at the He-Ne focal volume with a 25 μm pinhole and recording the radial location and scattered light signal at each location. The profiles are plotted and compared for concentricity. Adjustments to the beam alignments are made accordingly. Figure 1 shows the mapped normalized intensity profiles of the green Ar-ion beam and the red He-Ne beam in the vertical direction. The concentricity of the beams is apparent in the figure. The beam waists are determined at the $1/e^2$ point to be 396 μm for the 514.5 nm Ar-ion beam and 81 μm for the 632.8 nm He-Ne beam. These compare to beam waist theoretical calculations of 398 μm and 55 μm respectively. Note that the He-Ne beam lies in the 95 percent or greater intensity region of the Ar-ion beam.

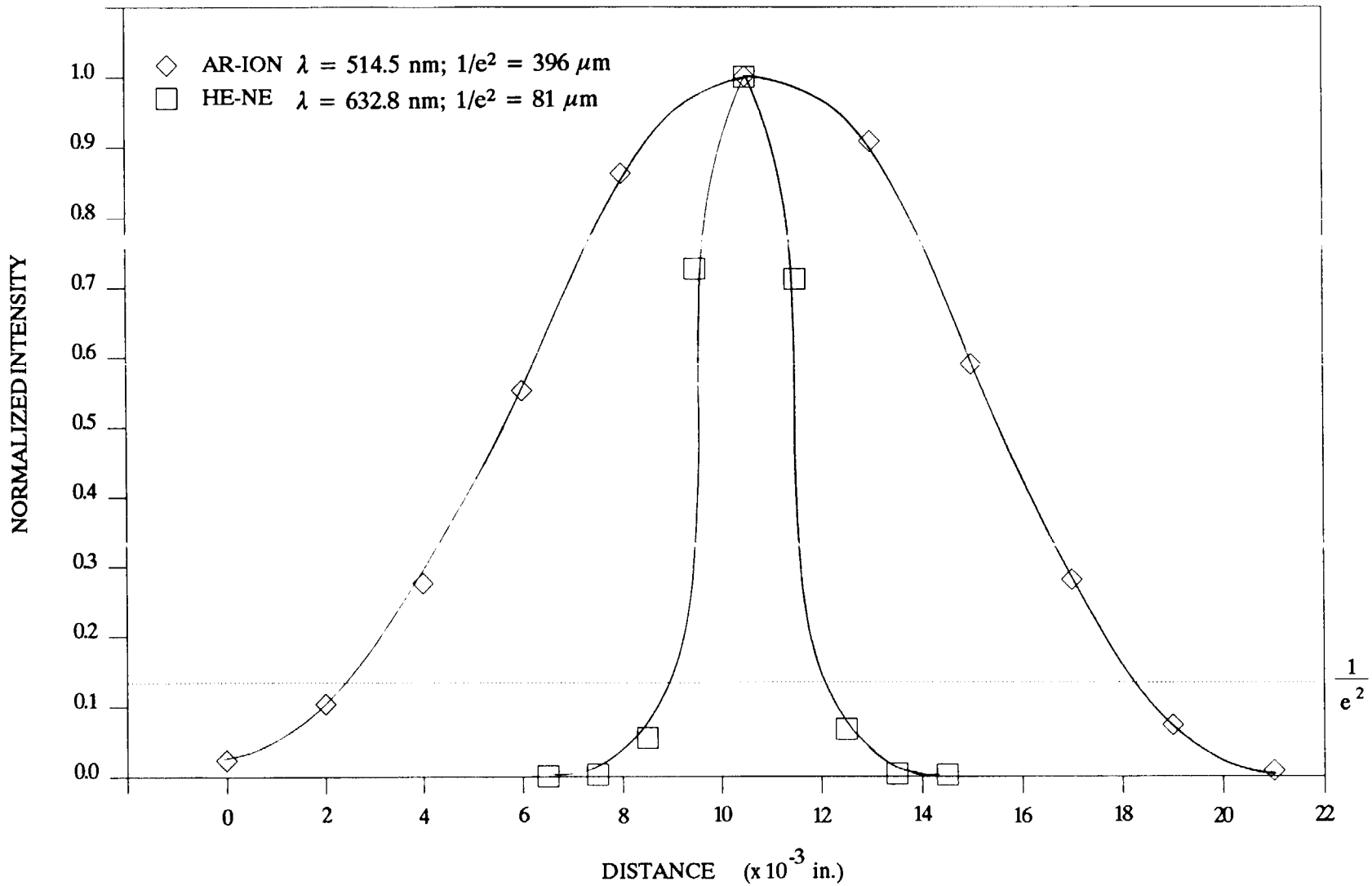

Figure 1: Profile Map of Ar-ion and He-Ne Laser Beams at the He-Ne Focal Volume Taken in the Vertical Direction.

The primary reason for using the two-color forward scatter technique developed by Wang and Hencken [1] is demonstrated by the oscilloscope trace in Figure 2. The left peak results from a particle passing through both the primary beam and the secondary concentric beam. The center and right peaks on the trace result from particles which passed through the primary beam but not the secondary beam. Accurate sizing of the particles that generated the second and third peaks is not possible because the particles could have passed through the primary beam in any region not covered by the secondary beam.

In the second step of the calibration process, pinholes of known diameters ranging from 5 μm to 150 μm were placed at the He-Ne beam focal location to correlate pinhole size with the intensity of the measured scattered light signal. Figure 3 is a graph of the measured pinhole scattered light and the normalized intensity curve as predicted by Mie theory for varying particle size. The Mie theory curve was generated for λ = 514.5 nm using a collection angle of ϕ = 1.29° with a $\Delta\phi$ = 0.92° corresponding to the experimental arrangement. Mie theory underpredicts the scattered light intensity for pinholes in the range of 5 μm to 25 μm and overpredicts for the 150 μm pinhole. The 50 μm and 100 μm pinholes appear to match the Mie theory. Work is in progress using a scanning electron microscope to examine the pinholes for roundness and to determine size accuracy. Adjustments to the pinhole calibration will then be made as required.

The last step of the calibration process involves testing the system with monodisperse droplets of known diameter. The calibration apparatus consists of a vibrating orifice droplet generator, a chamber to contain the aerosol and a tube to direct the droplets into the sampling region. The droplet generator produces a monodisperse

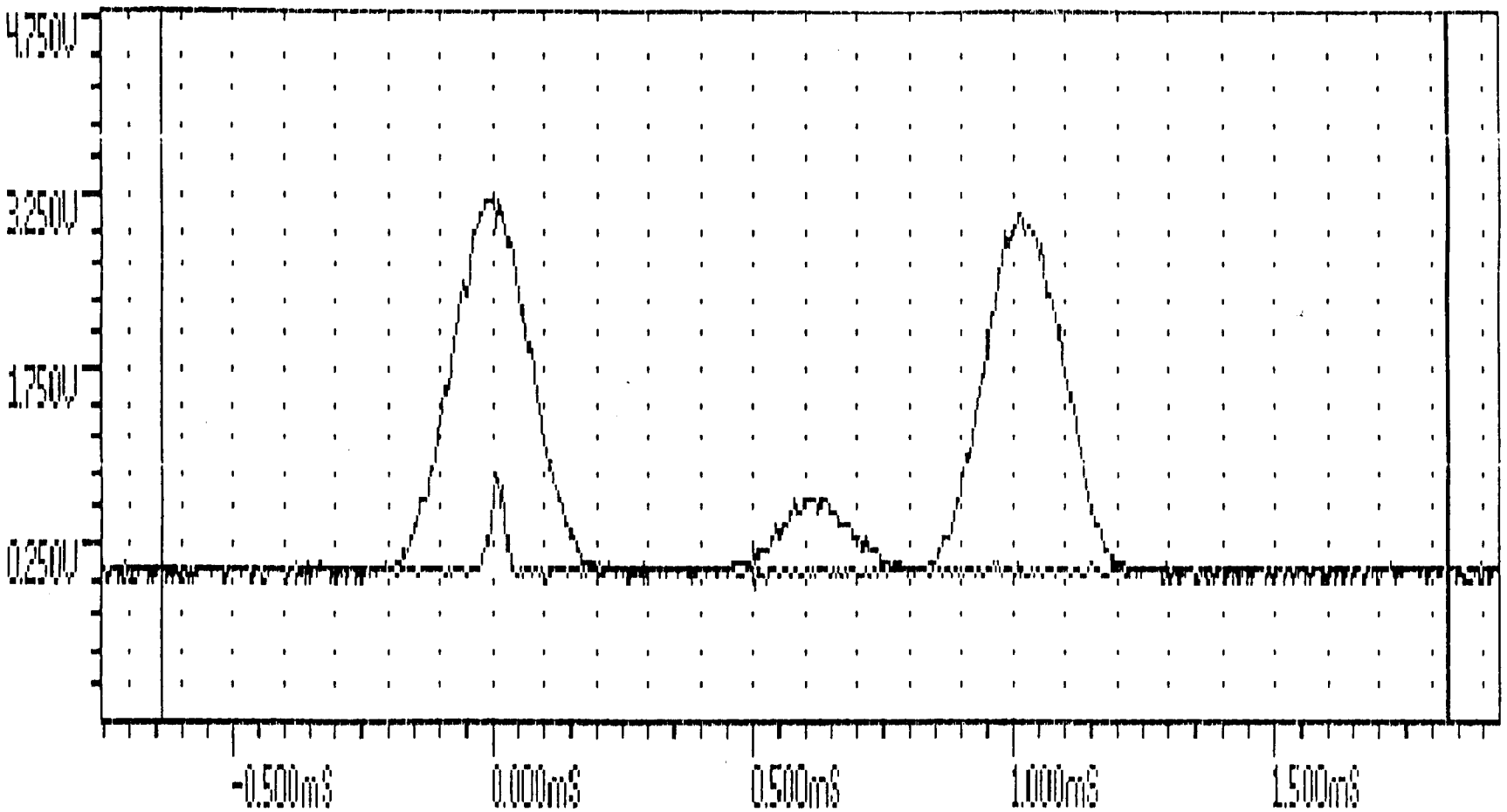

Figure 2: Oscilloscope Trace of Multiple Particles Passing Through the Laser Beam Focal Volume. Left Peak is Acceptable in Two-Color Particle Sizing Technique.

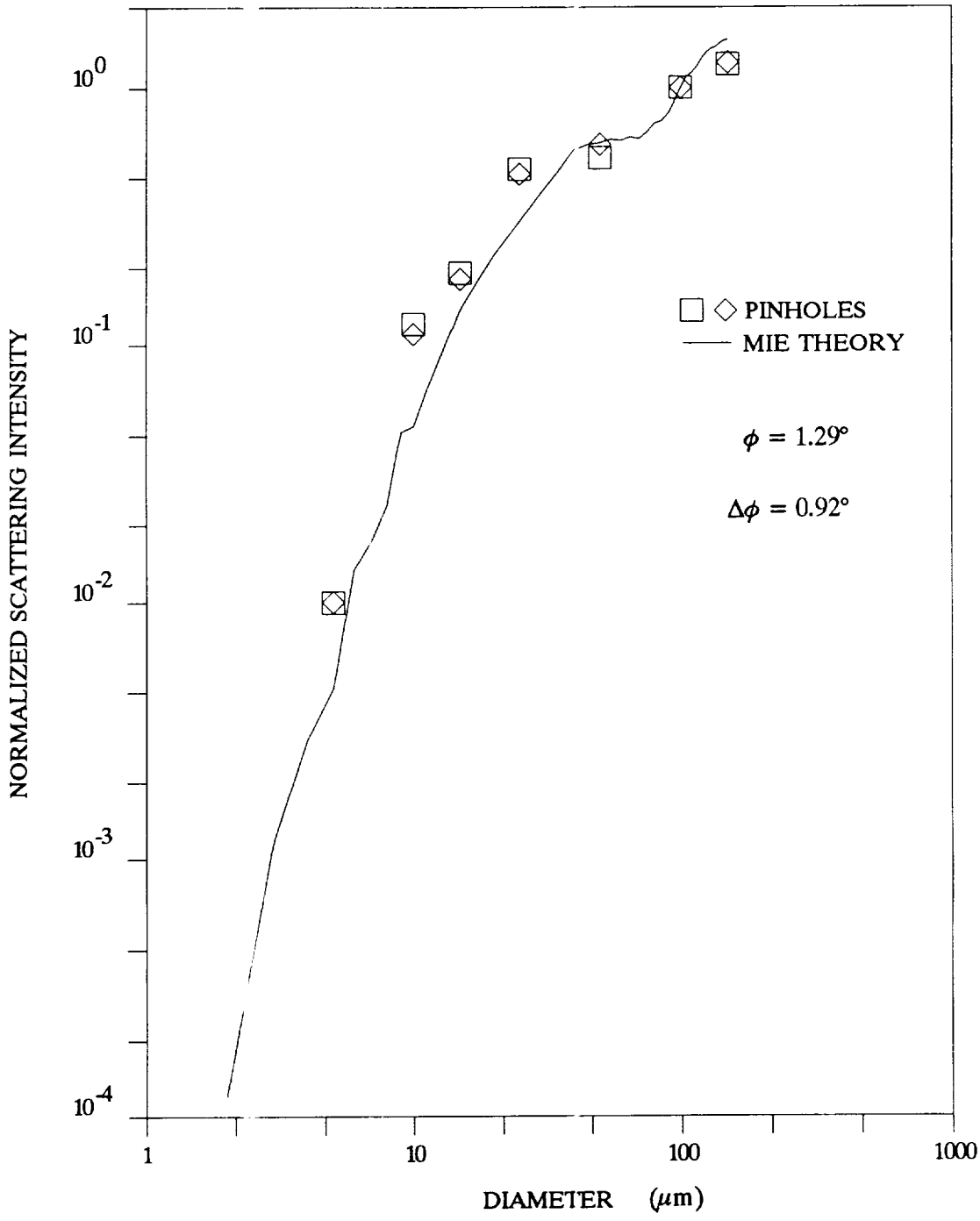

Figure 3: Mie Theory Correlation and Pinhole Calibration.

stream of droplets which is diffused into an aerosol by a stream of air. The airstream carries the droplets through the chamber, up the tube to the sampling region. To facilitate the calibration process, the burner is rotated out of place and the droplet generator slid into the burner location. Figure 4 is a schematic of the layout. Distilled water is used as the working fluid in the droplet generator.

The initial attempt to measure water droplet diameters dynamically with the forward-scatter system produced particle size measurements somewhat smaller than expected, based on calculations provided by the manufacturer of the vibrating orifice droplet generator. Subsequent checks of the droplet generator using digital camera imaging techniques demonstrate that the two-color forward scatter technique is working properly. Figure 5 is a photographic image of the digital camera output. The particle size ranges measured with the digital camera and the two-color scatter technique are shown in Figure 6. Mean droplet diameters were 82 μm with a standard deviation of ± 13 μm for the two-color scatter system and 75 μm with a standard deviation of ± 3 μm for the imaging measurements.

Varying the operating parameters of the droplet generator produced the results shown in Figure 7. These results demonstrate that the two-color forward scatter system is capable of measuring particles in the range of 10 μm to 200 μm as anticipated.

Particle velocity is determined by dividing the primary beam diameter (396 μm) by the time-of-flight measurement. The time-of-flight is determined from the signal intensity profile which is recorded as a function of time. The time width of the signal peak is measured at the $1/e^2$ signal intensity drop-off points. Figure 8 is a scattergram of the velocities calculated for the water droplets from the size calibration experiments.

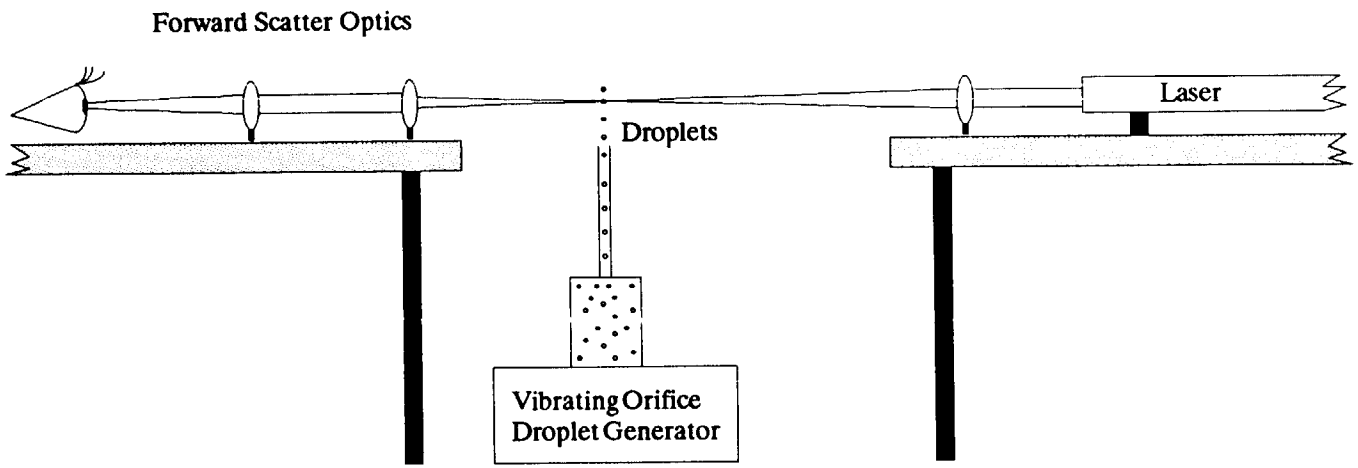

Figure 4: Schematic of Droplet Generator Calibration Apparatus in System.

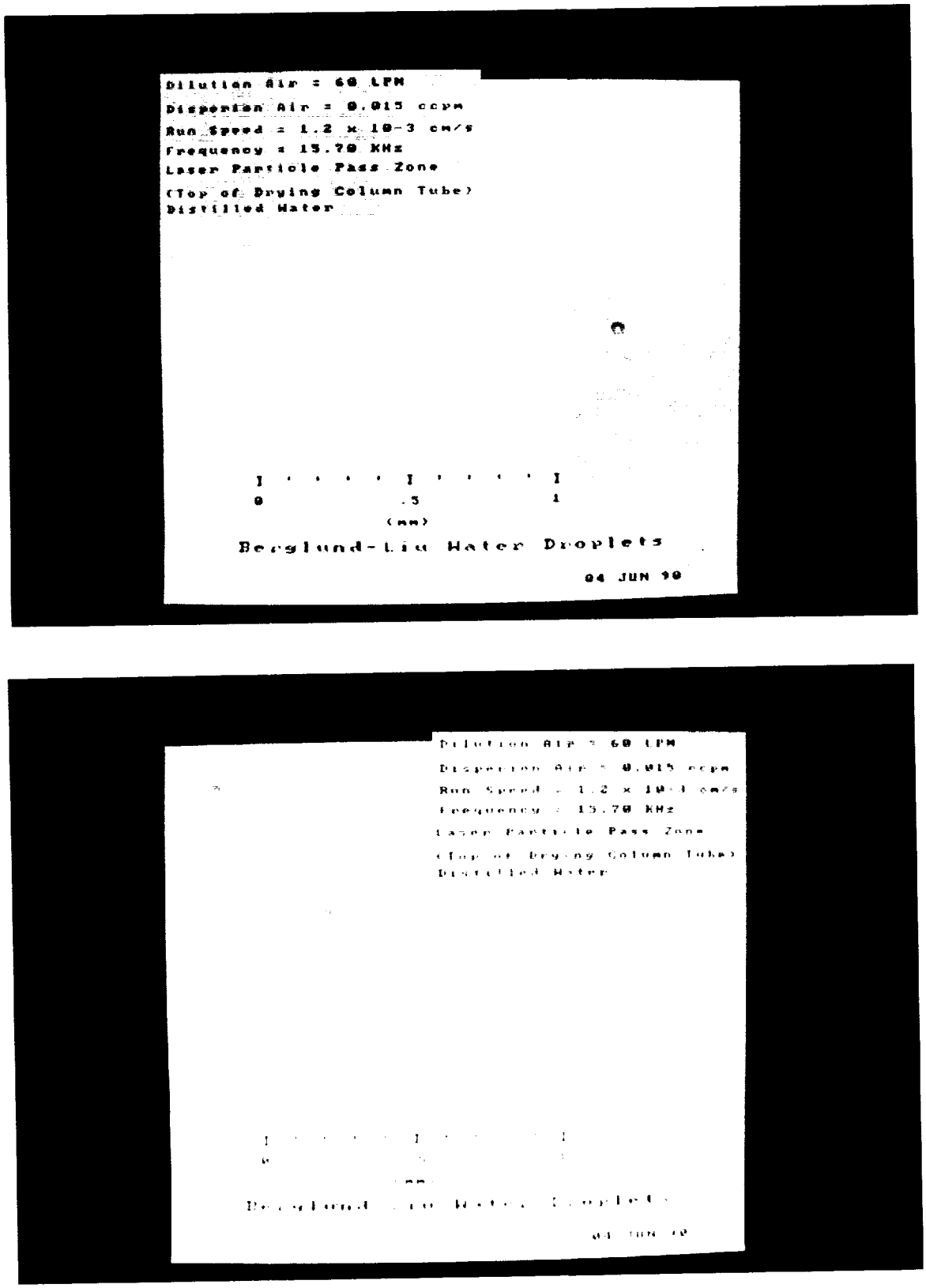

Figure 5: Photographic Images of Water Droplets Taken with a Digital Camera.

ORIGINAL PAGE IS
OF POOR QUALITY

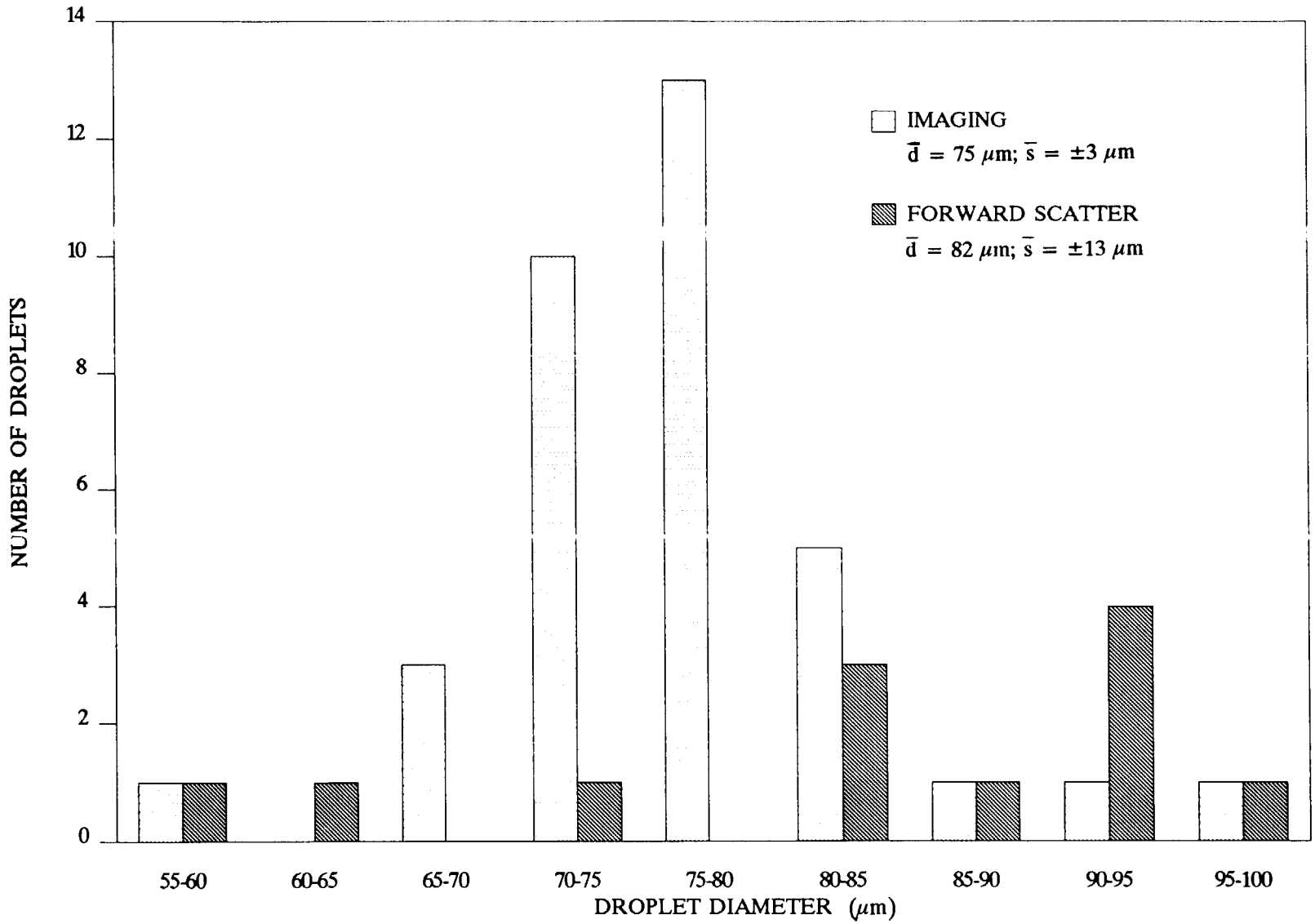

Figure 6: Water Droplets Measured by Digital Camera Imaging Technique and Two-Color Forward Scatter.

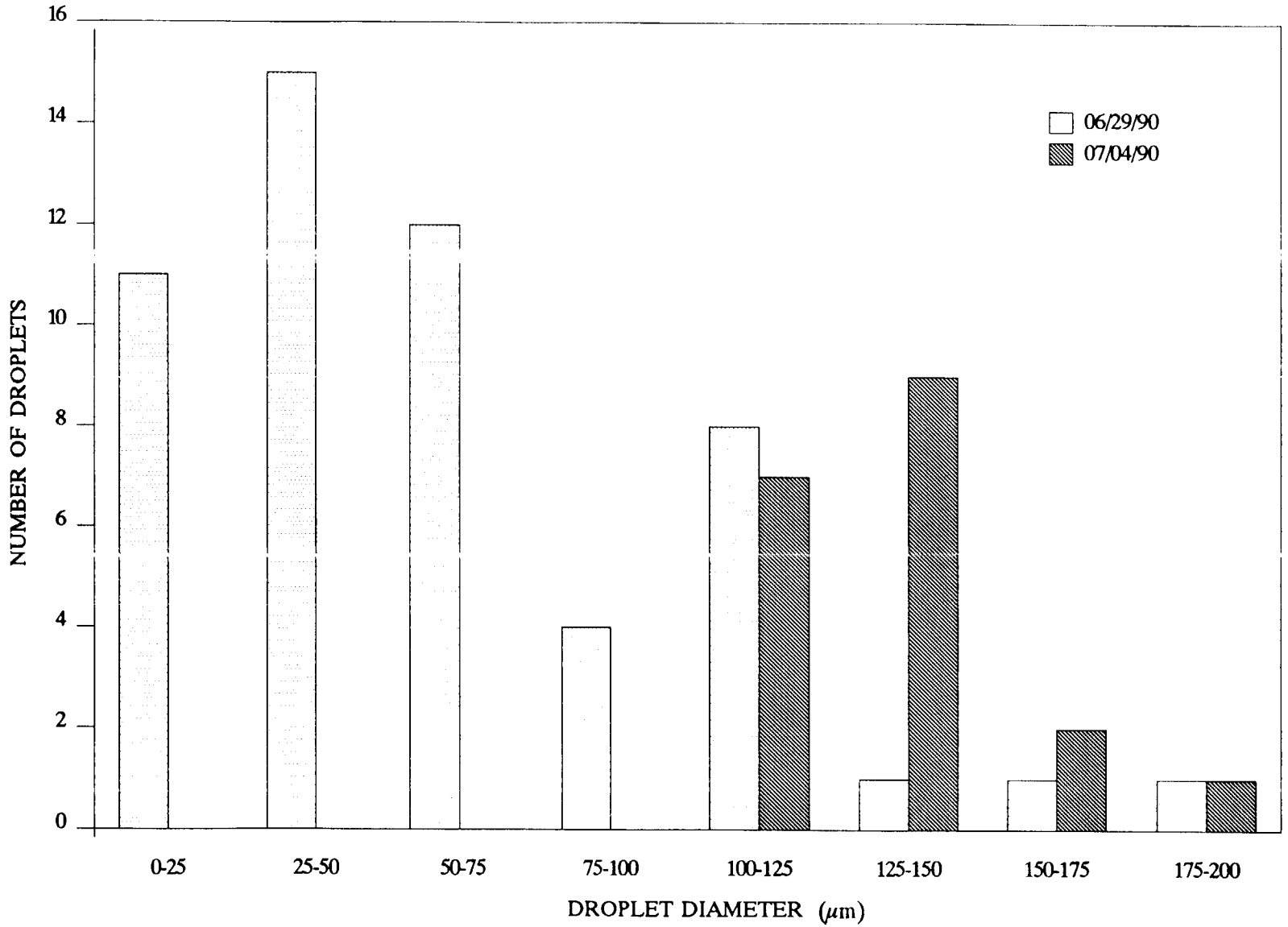

Figure 7: Water Droplet Measured by Two-Color Forward Scatter Technique.

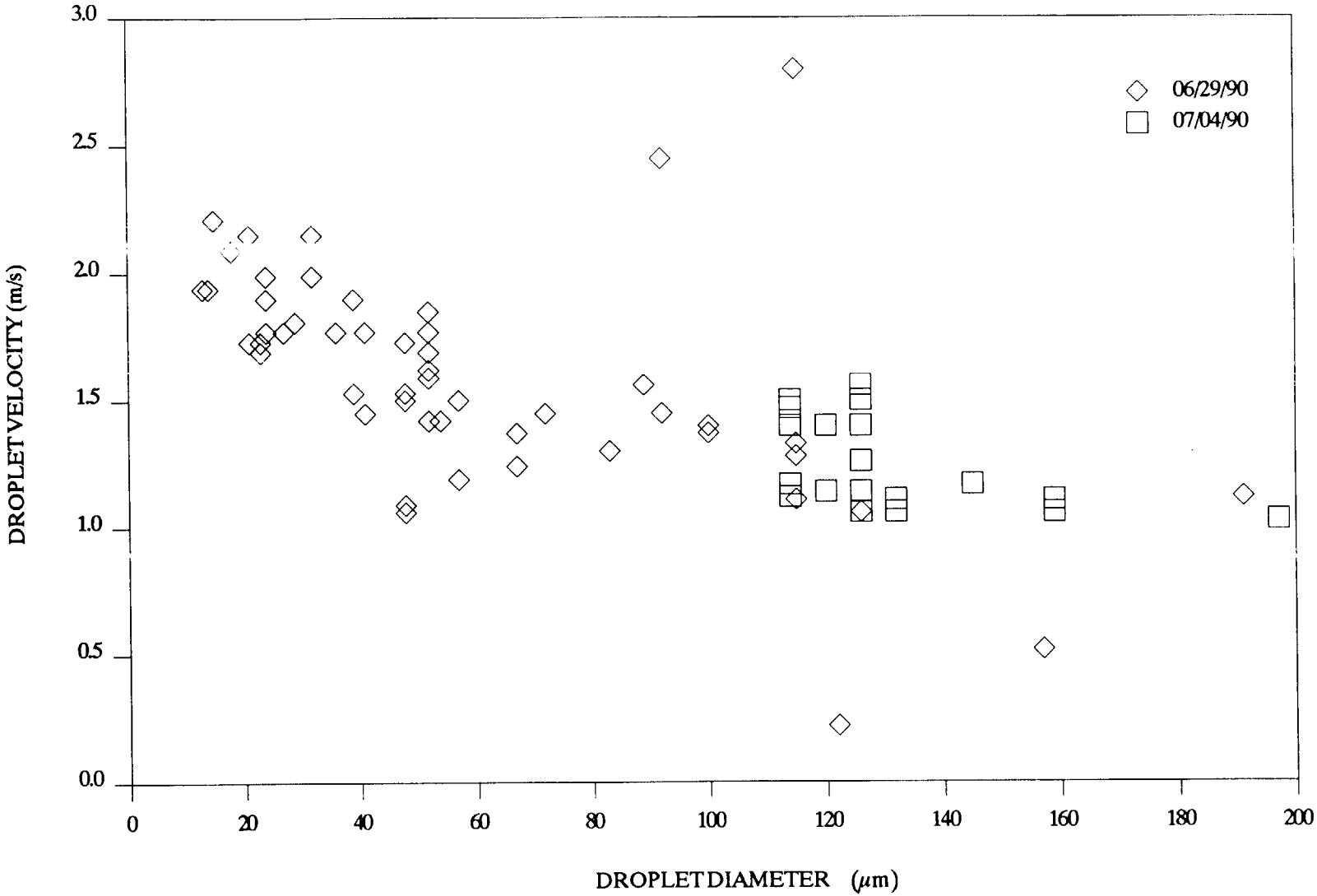

Figure 8: Scattergram of Water Droplet Velocities Measured Using Two-Color Forward Scatter Technique.

Signal Conditioning

The electronics for signal conditioning are in place and operational with the exception of the logarithmic amplifier. Troubleshooting of problems with the logarithmic amplifier is in progress.

Data Acquisition System

The data acquisition and analysis programming has been completed as of this time with plans to continue testing the validation code through the use of the vibrating orifice droplet generator.

Potential problems that were considered for the data acquisition system are demonstrated with the oscilloscope traces shown in Figures 9 through 12. Figure 9 shows misaligned peaks. Closely spaced multiple particles passing through the system produced no leading edge on the one acceptable peak in Figure 10. Accurate determination of the time-of-flight in this instance is difficult. Of the three peaks associated with a trigger signal, (Figure 11), the left and right peaks have no trailing edges thus rendering them unacceptable. The center peak is acceptable and would be recorded. Misshapen peaks, such as that shown in Figure 12, are also discarded by the data acquisition system. Figure 13 is an oscilloscope trace of an acceptable signal. Note the Gaussian shape of the primary beam trace and the centering of the secondary beam trigger trace. The sharp peak of the secondary beam trace is an indication that the particle passed through the center of both beams.

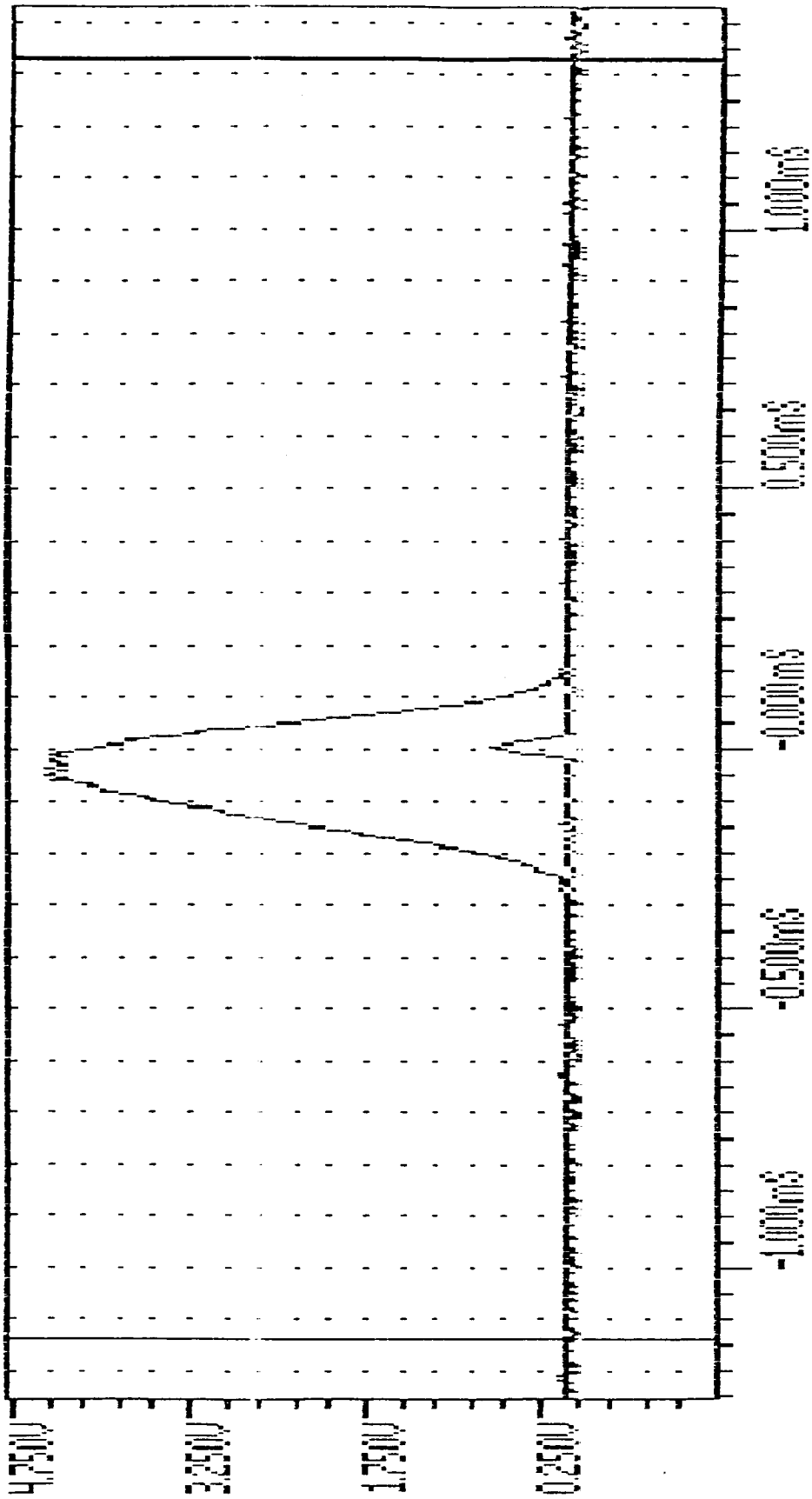

Figure 9: Oscilloscope Trace of Misaligned Peaks.

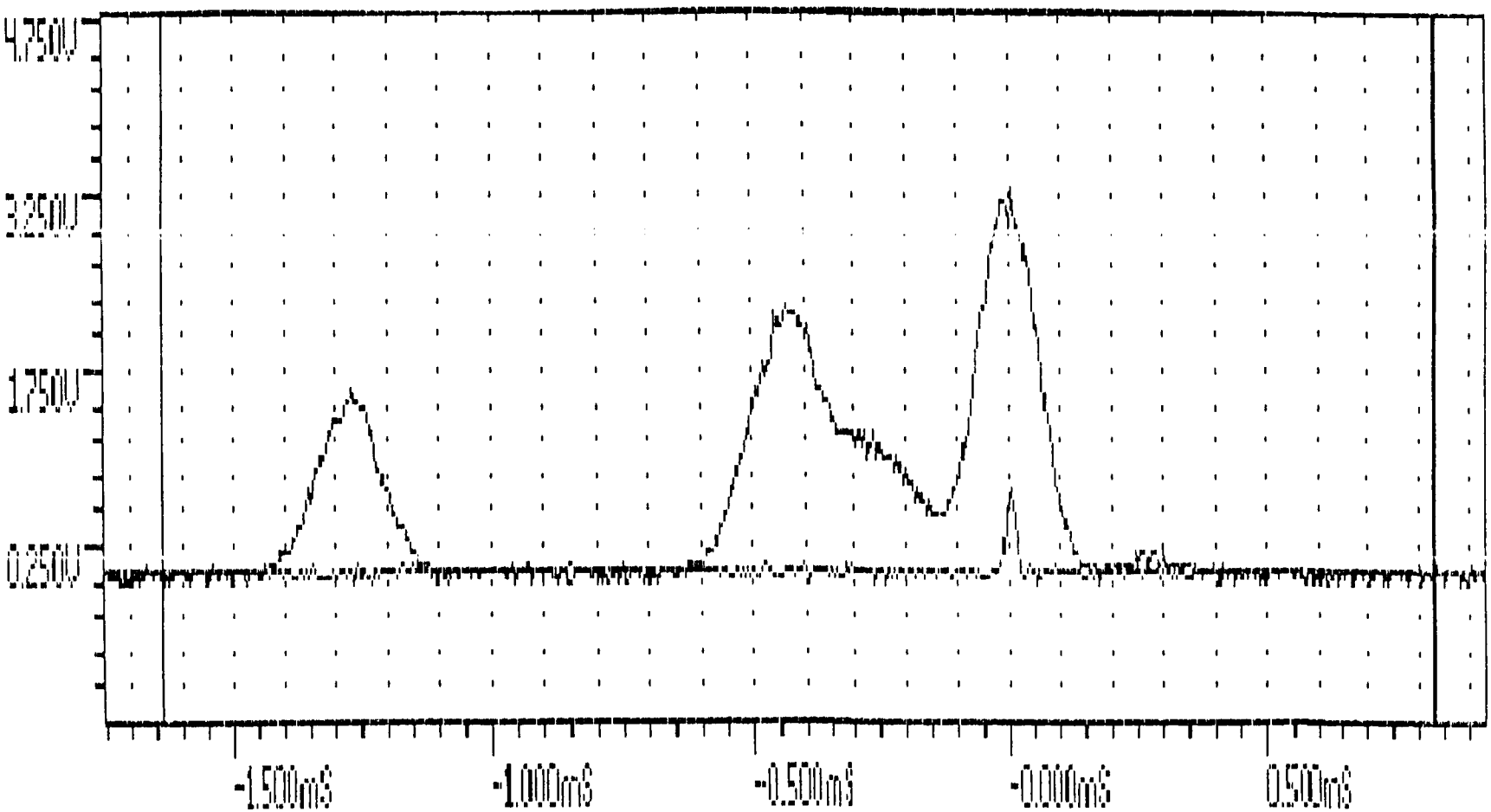

Figure 10: Oscilloscope Trace of No Leading Edge for Acceptable Particle.

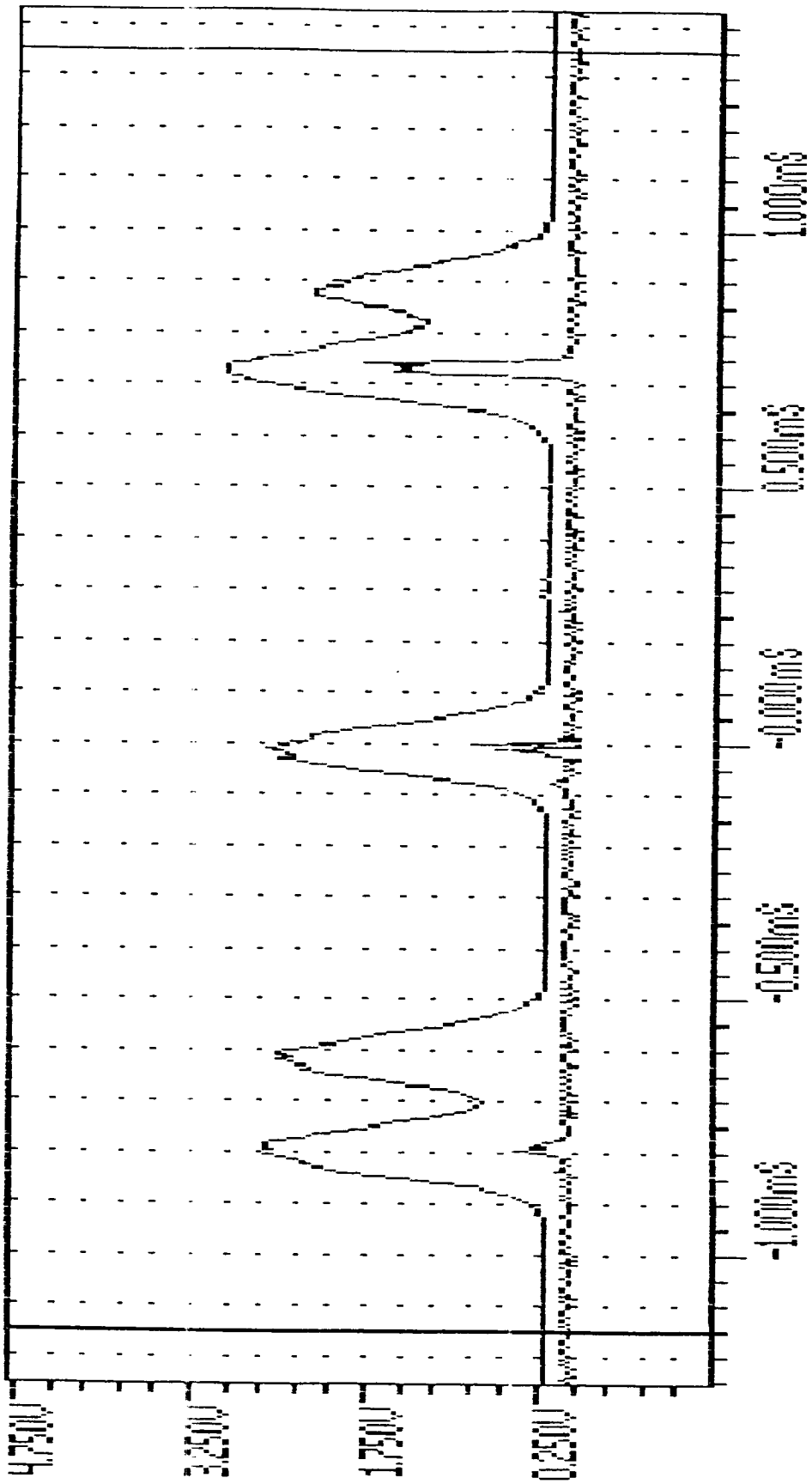

Figure 11: Oscilloscope Trace of No Trailing Edge for Acceptable Particle.

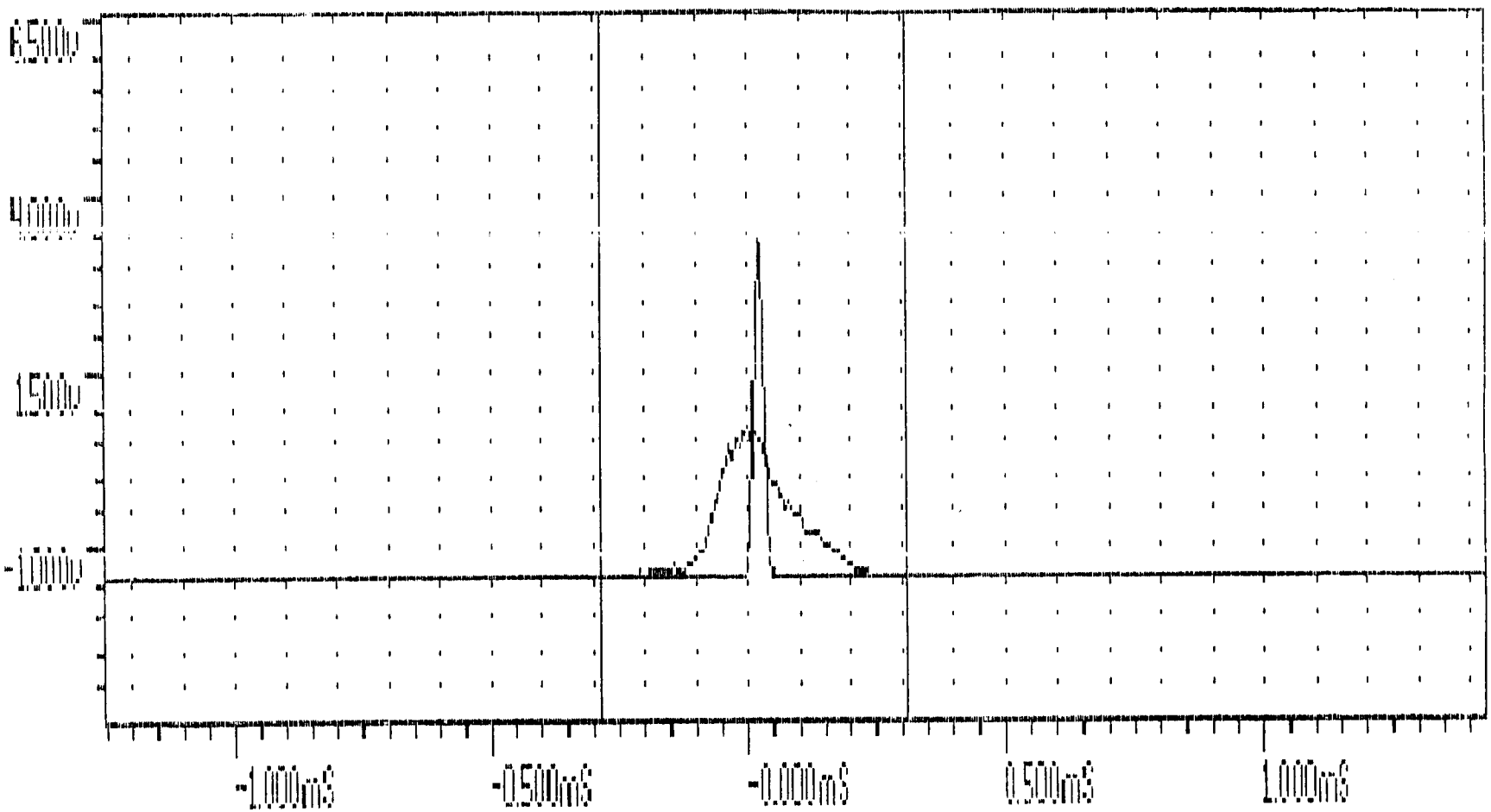

Figure 12: Oscilloscope Trace of Skewed Particle Light Scatter.

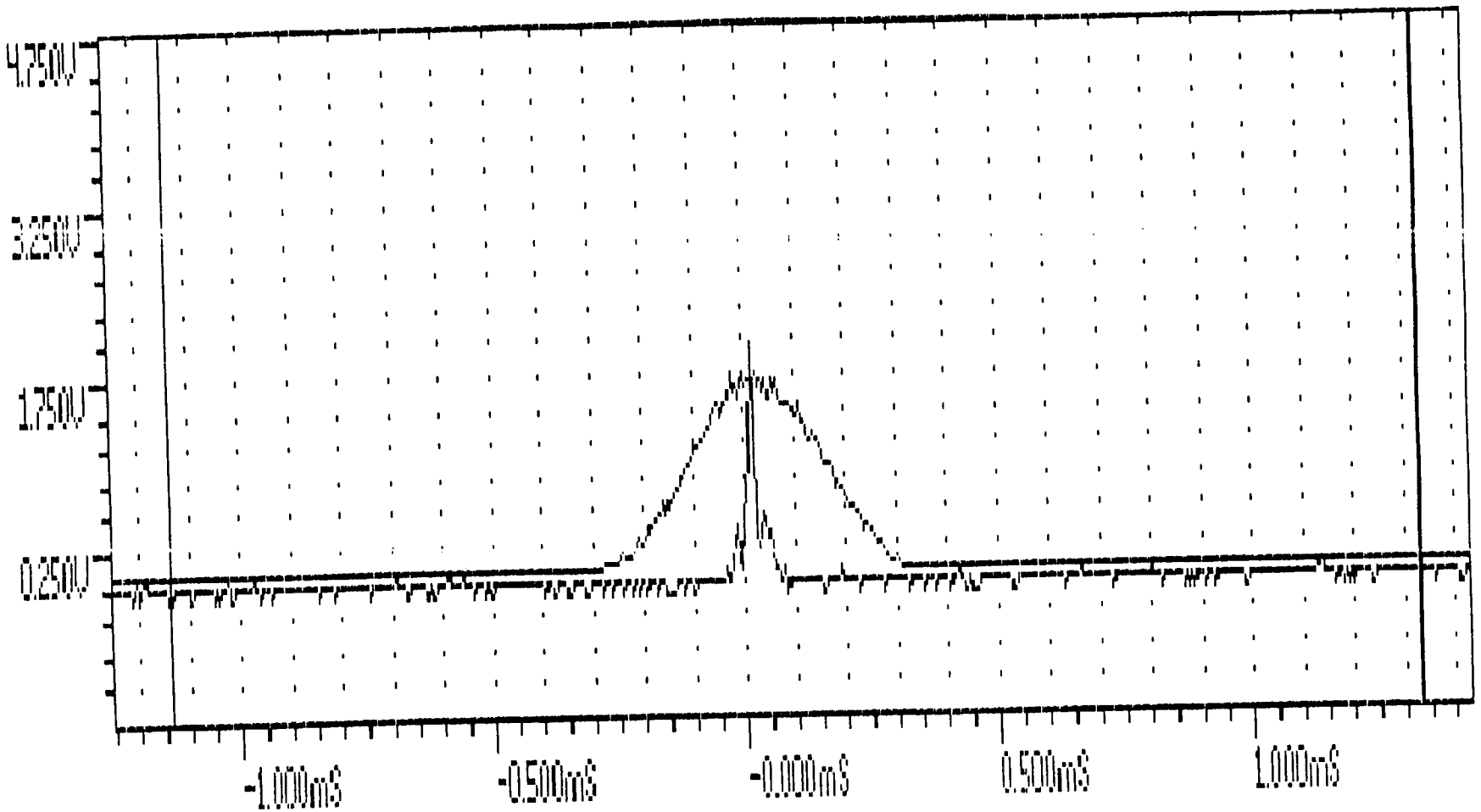

Figure 13: Oscilloscope Trace of Acceptable Particle for Two-Color Particle Sizing Technique.

BURNER AND SPRAY RIG SYSTEM

Burner System

Details of the laminar burner, the translation system, the slurry delivery system and the slurry atomization system were reported in the January 1990 Semi-Annual Report.

Subsequent to being damaged in a mishap caused by a faulty seal, the non-premixed laminar burner has been reassembled using both O-rings and a sealant to prevent another leak in the fuel manifold. This seal has been tested to a static pressure of 40 psig, far above the minimal pressures encountered in operation. Since then, no further leakage problems have been encountered.

The burner has been tested over an array of conditions ranging from equivalence ratios of 0.2 to 1.0 and oxygen mass fractions of 0.23 up to 0.4. Methane was the fuel and an O_2/N_2 mixture the oxidant. It was found that operation at near-stoichiometric or richer conditions resulted in a large single flame instead of the 72 small diffusion flames. Flame temperatures and product gas composition have been predicted using the NASA CEC-76 combustion code (Figures 14 and 15).

The theoretical temperature values will be compared to measurements using Beryllium oxide coated Pt-Pt-10%Rh thermocouples [2]. Radial measurements will also be taken at various axial locations to determine the product gas temperature uniformity.

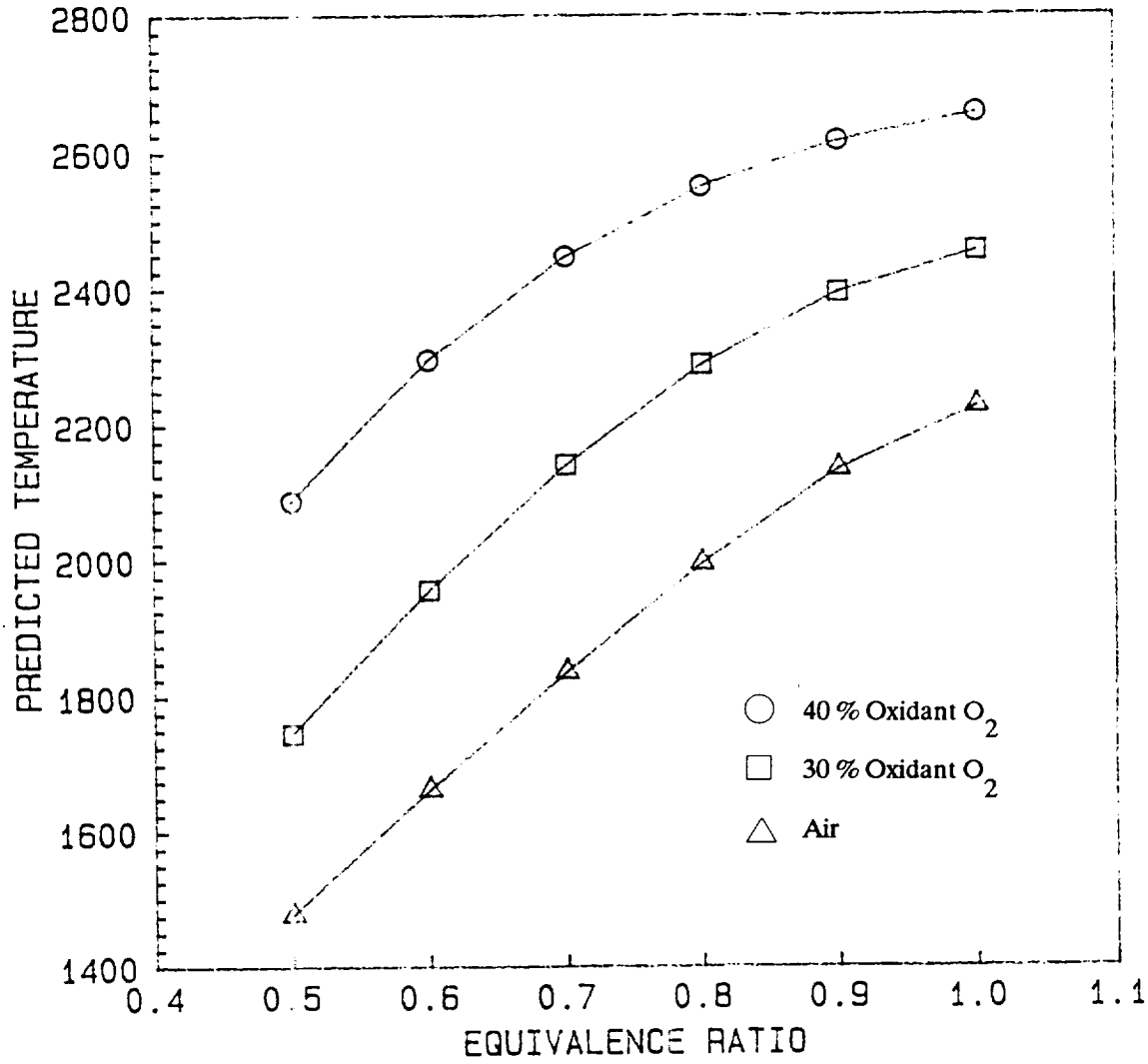

Figure 14: Plot of Predicted Flame Temperature vs. Equivalence Ratios For Given Oxidant O_2 Mass Fractions.

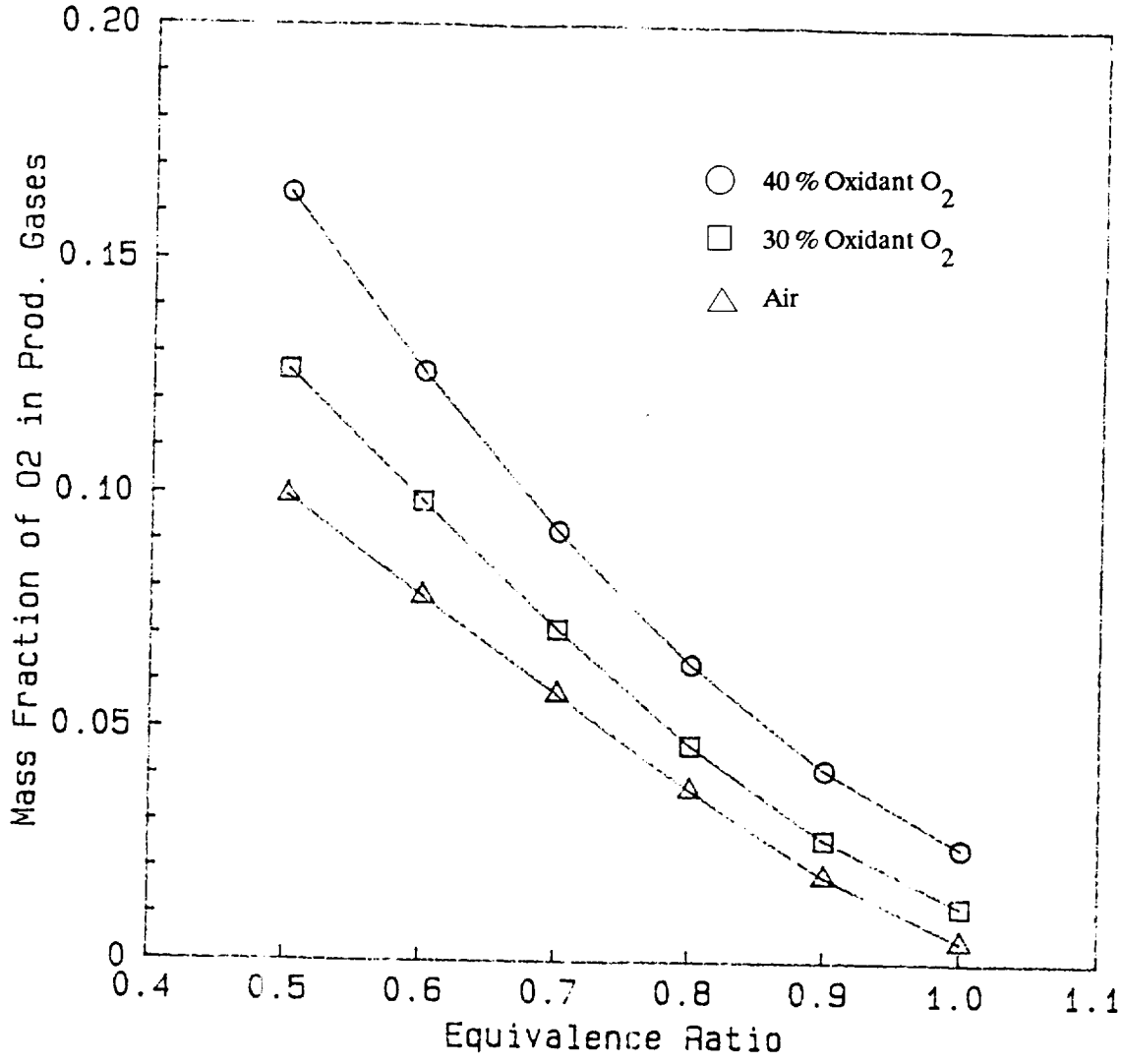

Figure 15: Plot of O_2 Mass Concentrations in Post-Flame Region vs. Equivalence Ratios for Given Oxidant O_2 Concentrations.

Flow Control System

The burner flow control system has been designed to permit independent control of flame stoichiometry and oxidant O_2 concentration. As can be seen in Figure 16, each of the three main gases, O_2, N_2, and CH_4, flows through a throttle valve and then branches to the appropriate rotameters. These individual flows are then adjusted with control valves downstream of the rotameters.

The pressure at each of the three main branching points is monitored with a sensitive absolute pressure gauge (Heise Solid-Front-C-54328). The pressures are then maintained at fixed values using the three throttle valves upstream of the rotameters. With choked flow at the rotameter outlet valve, the rotameters then operate at constant pressure independent of the burner pressures farther downstream.

The rotameters were calibrated using both a gas flowmeter (Singer Model 802) and a bubble meter. The volumetric flowrates were then converted to mass flowrates and calibration curves were generated using a third order polynomial fit. A typical rotameter calibration curve is shown in Figure 17.

A micro-manometer (Gilmont model G-1500-A) is used to measure the pressure drop across the center burner tube that carries the slurry droplets. Since the flow through this tube is laminar, the average velocity is linearly proportional to the pressure difference between the atomization chamber and the ambient. Through the use of a ball valve on the chamber vent line, this pressure drop and the flowrate of the central tube can be controlled.

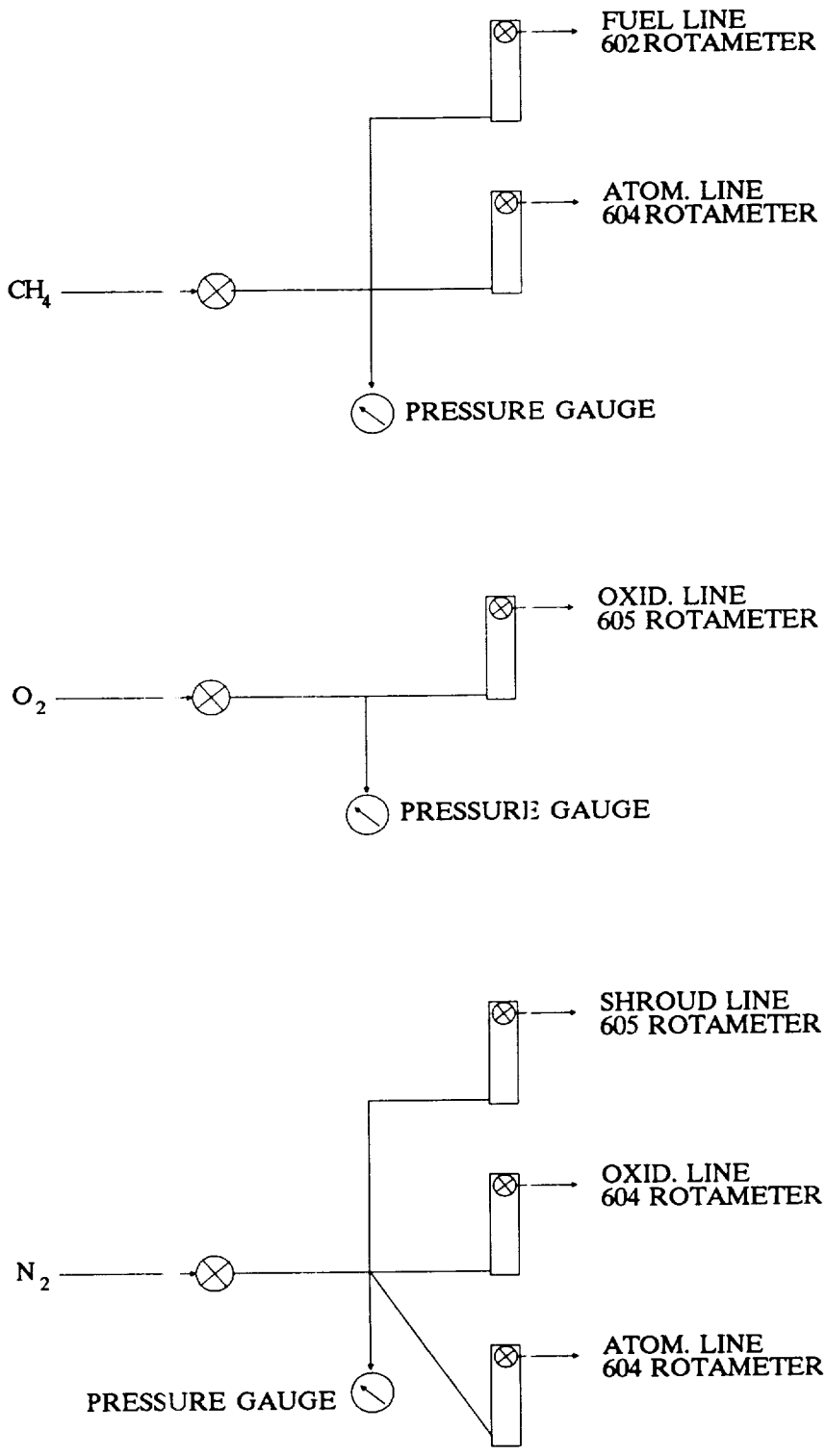

Figure 16: Schematic of Burner Flow System.

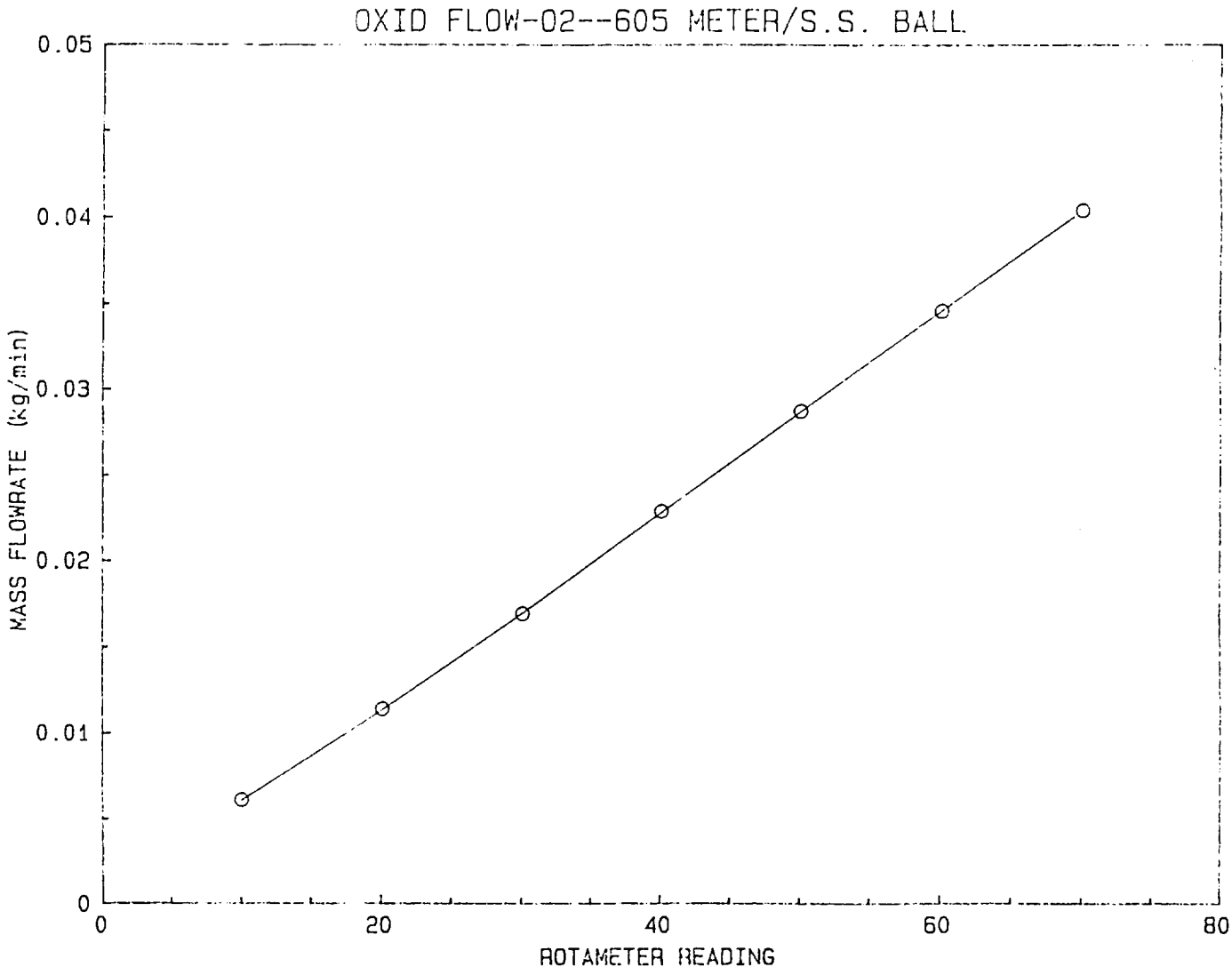

Figure 17: Calibration Data and Third Order Polynomial Fit for a Typical Rotameter.

Slurry Atomizing System

Following a series of burner shakedown tests, work was begun with the TRW, Aerojet, and Sun slurry formulations provided by NASA-Lewis. The Sun mixture has proved workable, creating no difficulties with the current atomization system. The TRW and Aerojet slurries have proved difficult to work with due to their viscous natures and will require a modified delivery system and chamber draining method.

Based on these factors, an initial database will be established using the Sun formulation. Later work on the TRW and Aerojet formulations will be performed upon redesign of the droplet atomization process.

RESULTS

Initial tests of the integrated system have been performed using JP-10 instead of a slurry formulation due to simplified handling procedures. Figures 18 through 23 show droplet size distribution plots and velocity-diameter scattergrams at various axial locations above the burner. The Sauter Mean Diameters were found to increase from 71.8 μm, at an elevation of 9.5 mm above the burner surface, to 112.4 μm at an elevation of 19.5 mm. This result is consistent with the smaller drops burning out first, with the larger droplets surviving longer. From Figures 18, 20 and 22, it can be seen that the majority of particles are between 20 and 100 μm in diameter, consistent with the anticipated performance of the atomization system. Figures 19, 21 and 23 illustrate the expected trend of decreasing velocity with increasing droplet size.

Numerous pictures of the slurry combustion process were taken at several burner operating conditions using the Sun slurry mixture. The photographs shown in Figures 24-26 were taken at an equivalence ratio of 0.5 and an oxidant O_2 mass fraction of 0.25 and illustrate a range of combustion characteristics. In all three figures, the RP-1 has ignited a short distance above the burner surface as shown by the glowing streaks in the particle flow. The two bright streaks in the droplet stream of Figure 25 are most likely due to the burning of aluminum. Figure 26 shows a micro-fragmentation process where a droplet has shattered into numerous smaller particles which continue to burn.

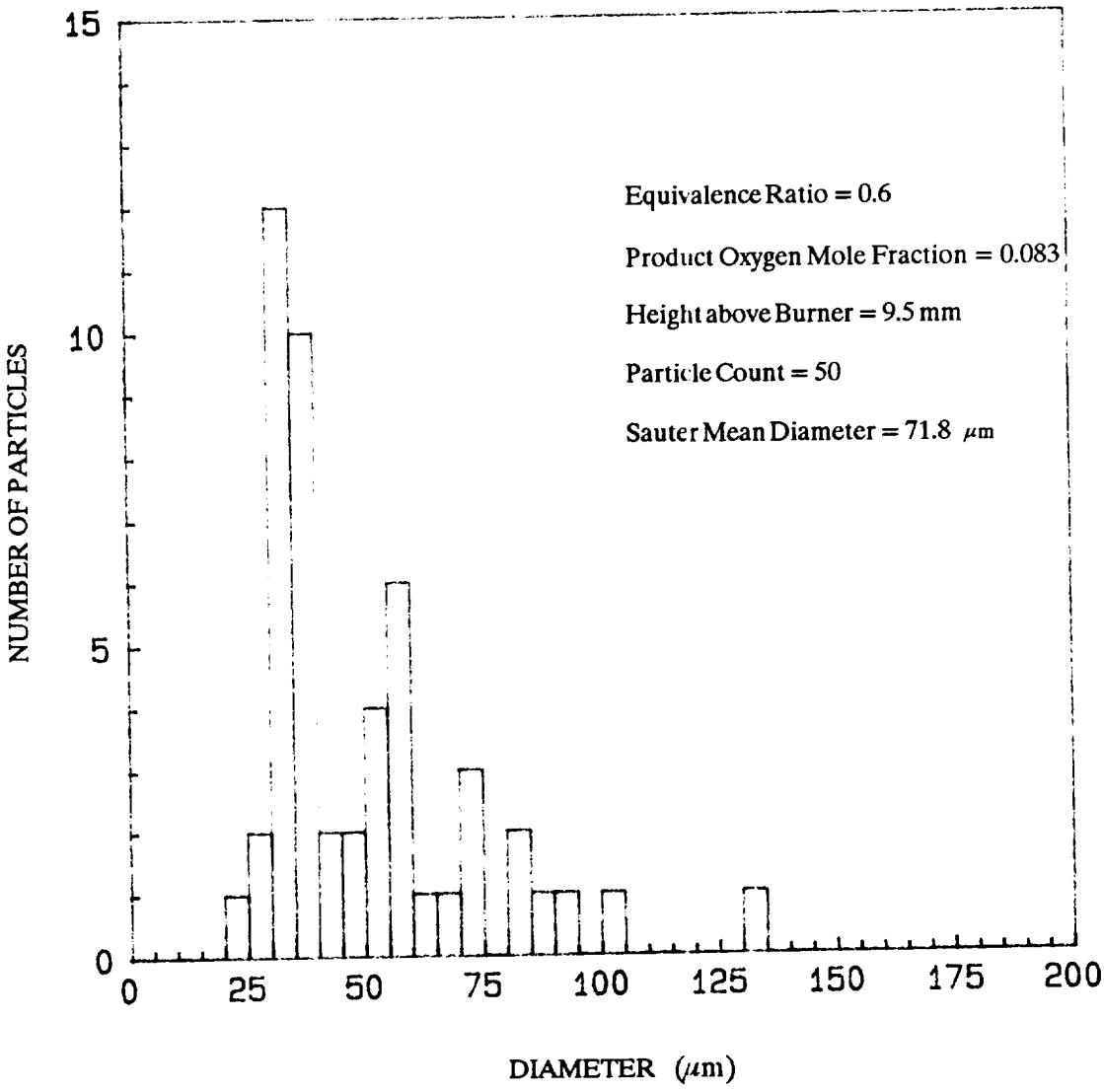

Figure 18: Size Distribution of JP-10 Droplets.

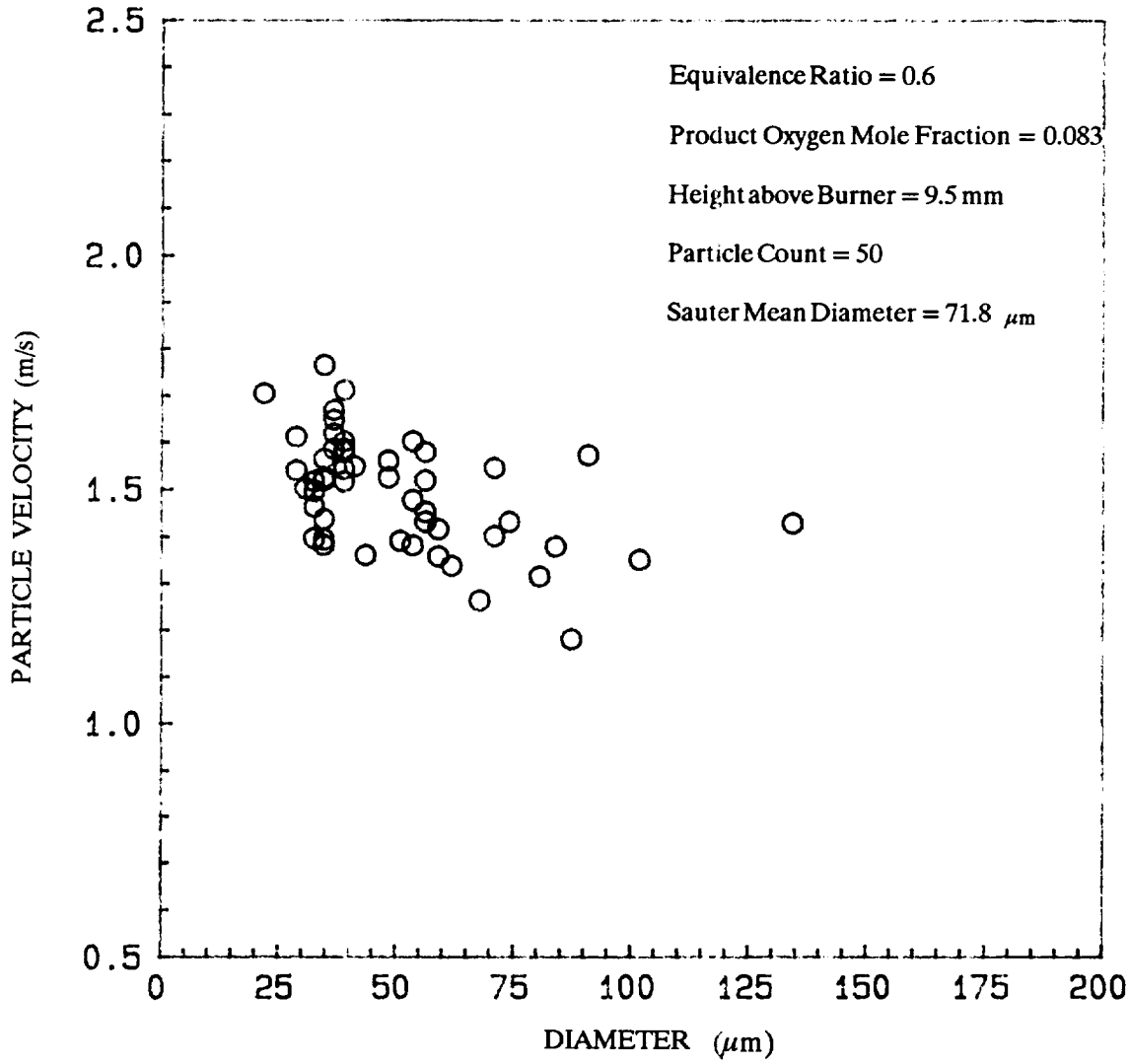

Figure 19: Velocity - Diameter Scattergram of JP - 10 Droplets.

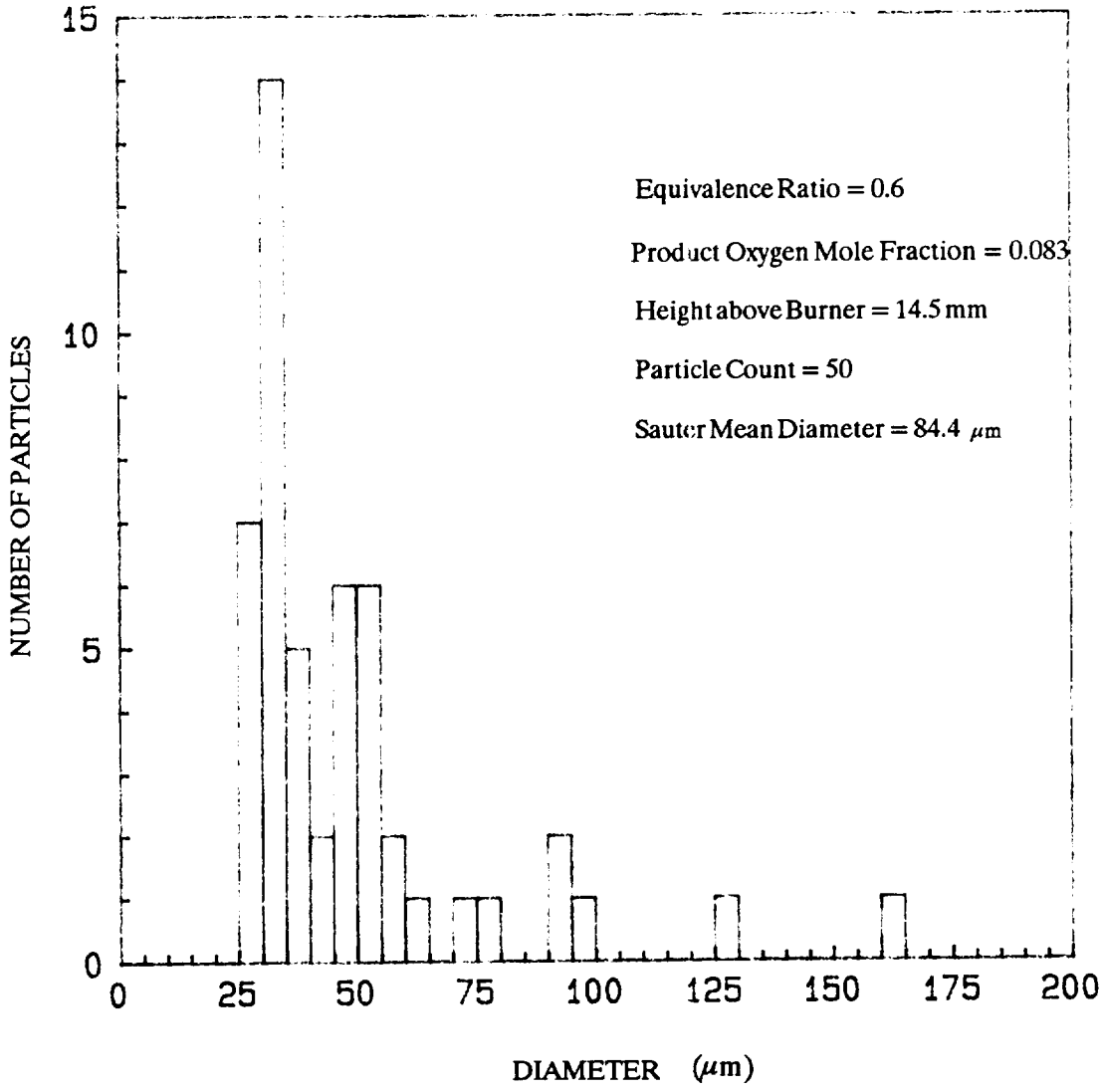

Figure 20: Size Distribution of JP-10 Droplets.

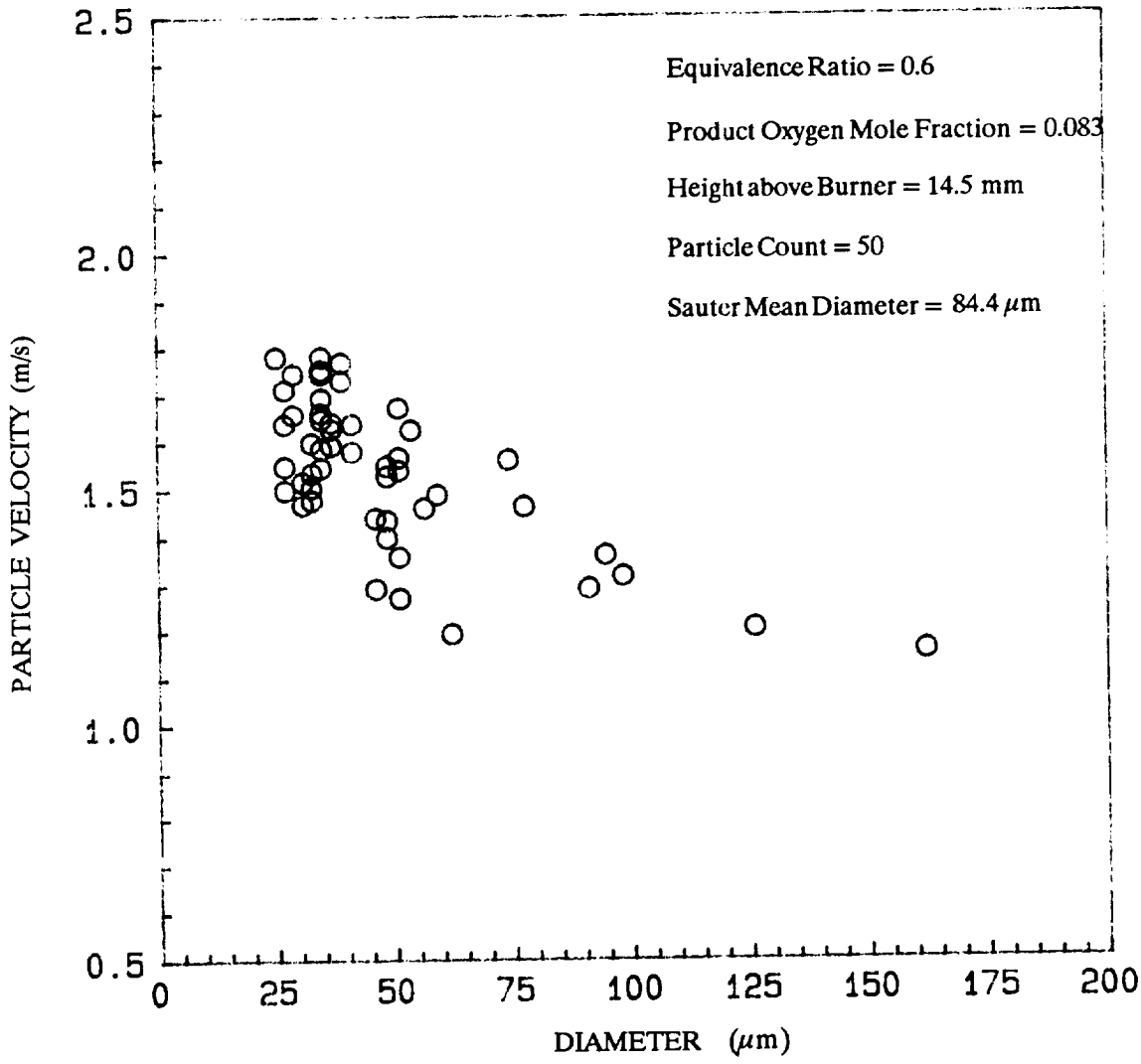

Figure 21: Velocity - Diameter Scattergram of JP - 10 Droplets.

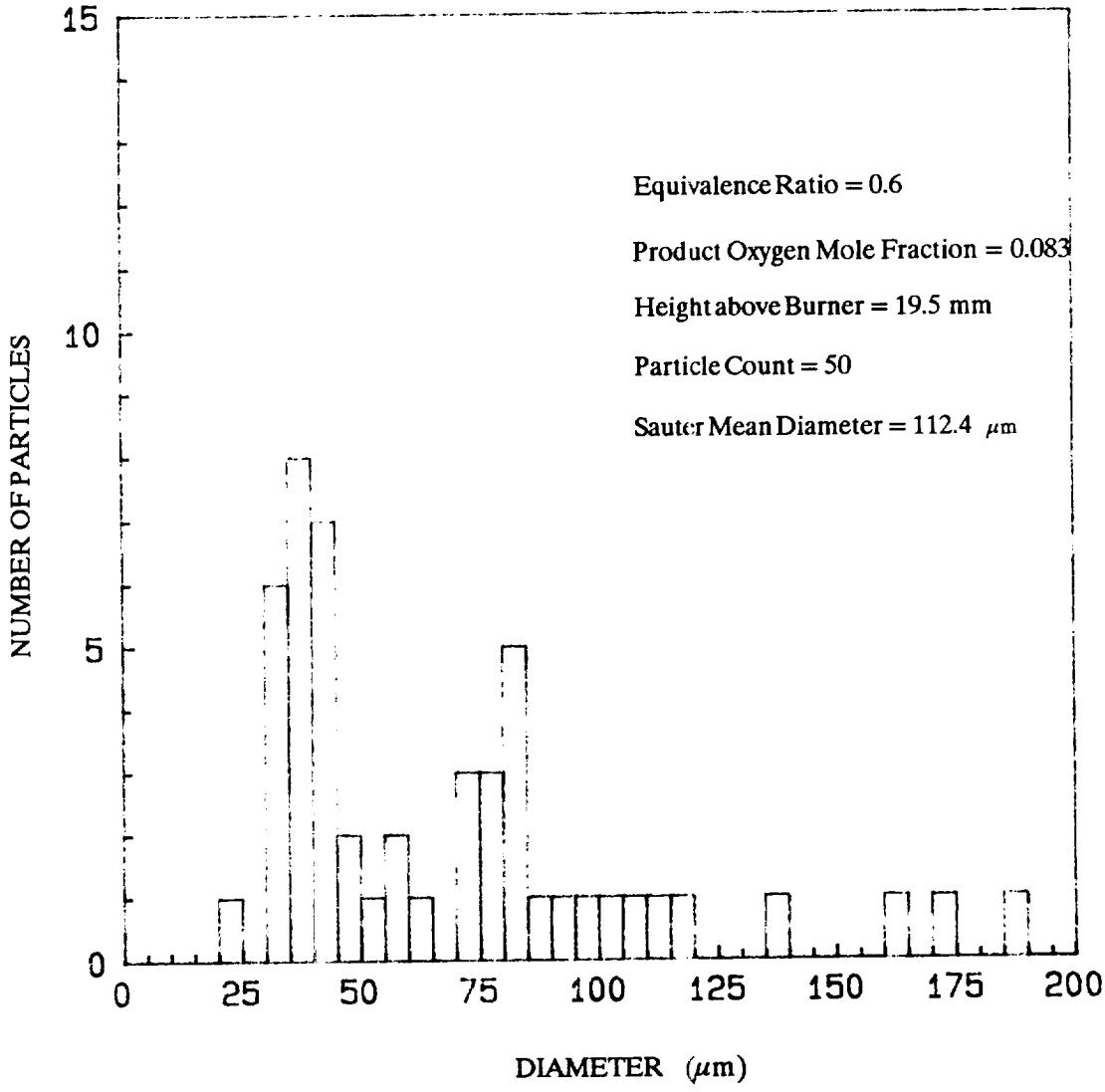

Figure 22: Size Distribution of JP-10 Droplets.

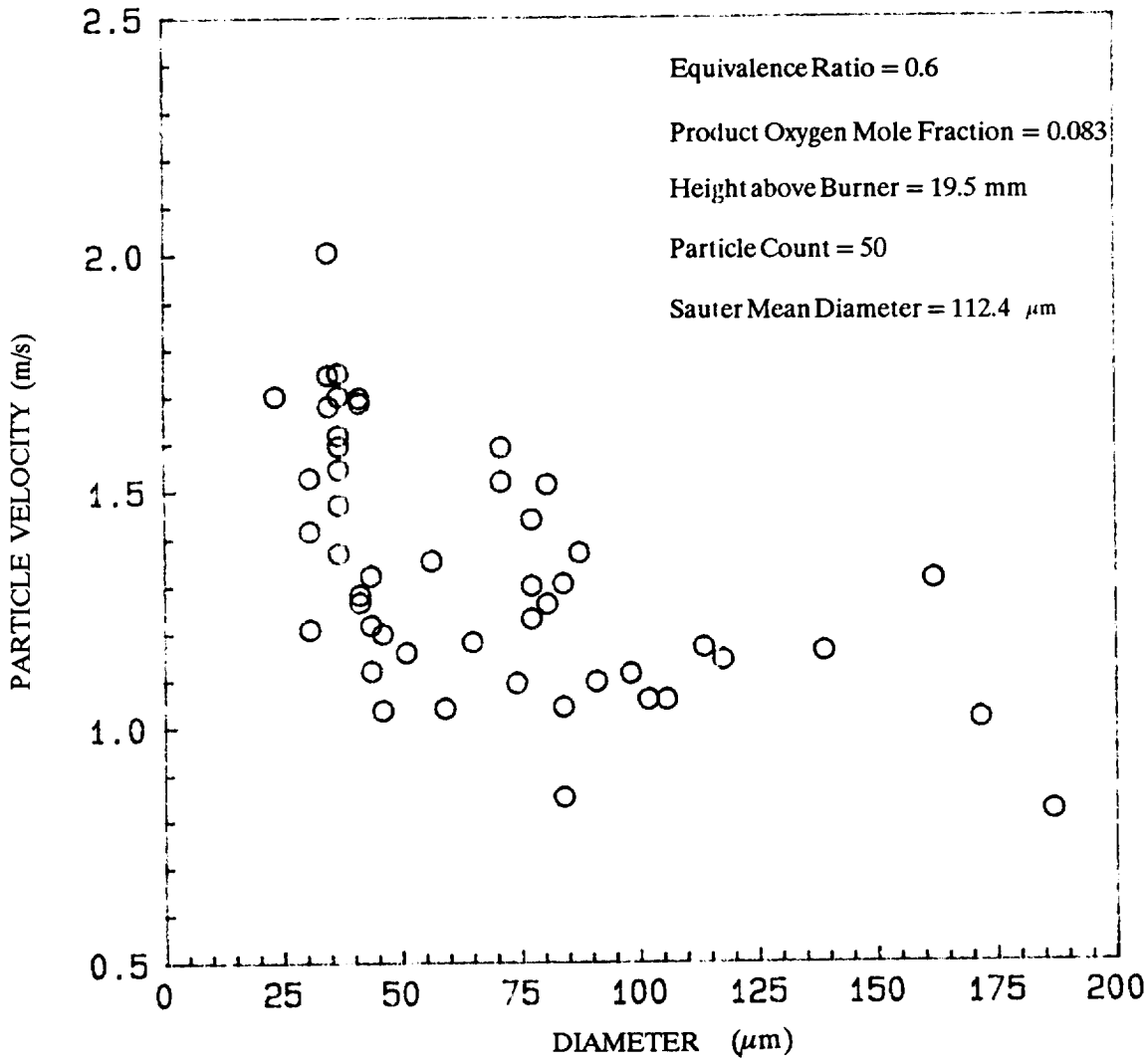

Figure 23: Velocity - Diameter Scattergram of JP - 10 Droplets.

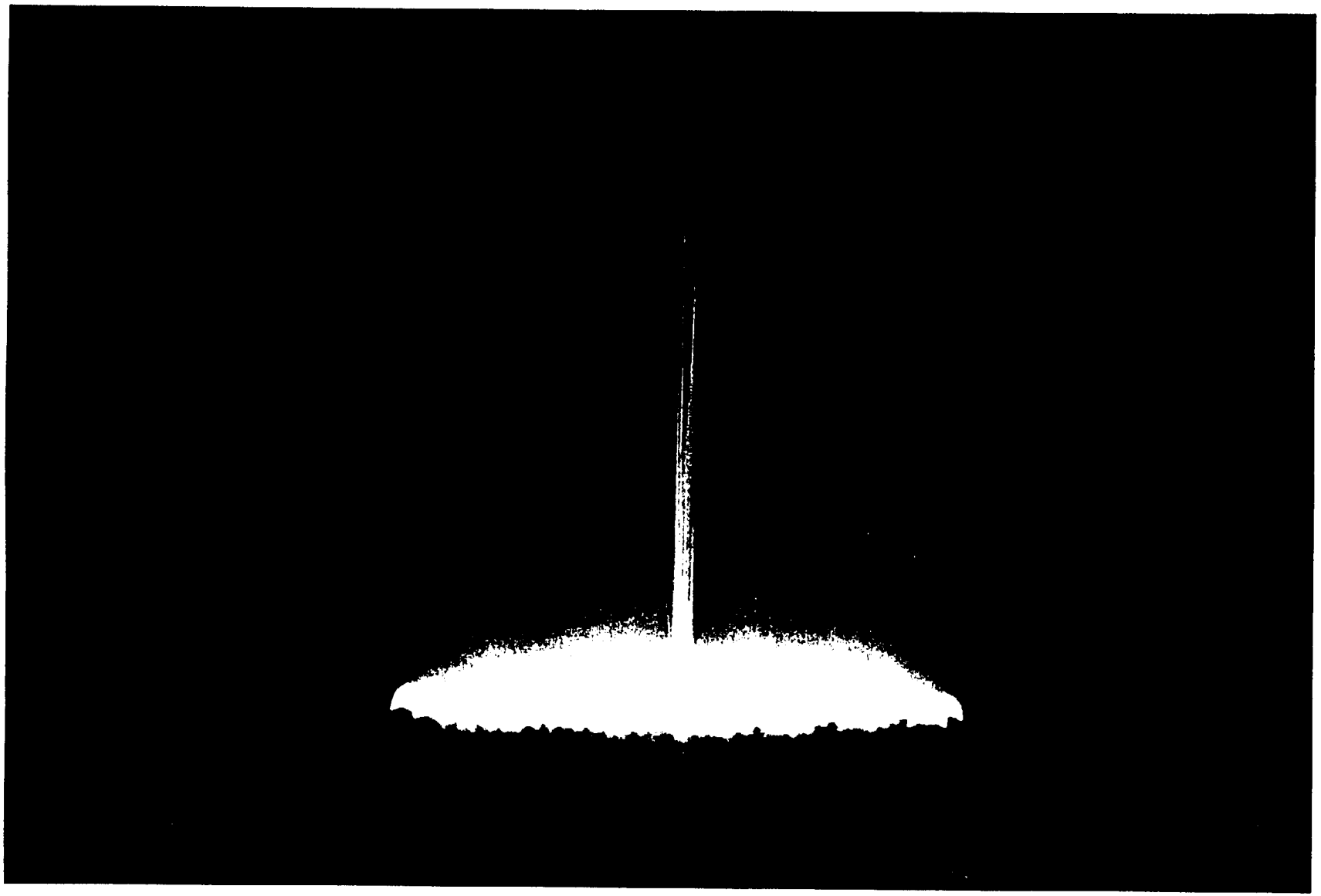

Figure 24: Sun Slurry Combustion at an Equivalence Ratio of 0.5 and an Oxidant O_2 Mass Fraction of 0.25 Showing only RP-1 Burning.

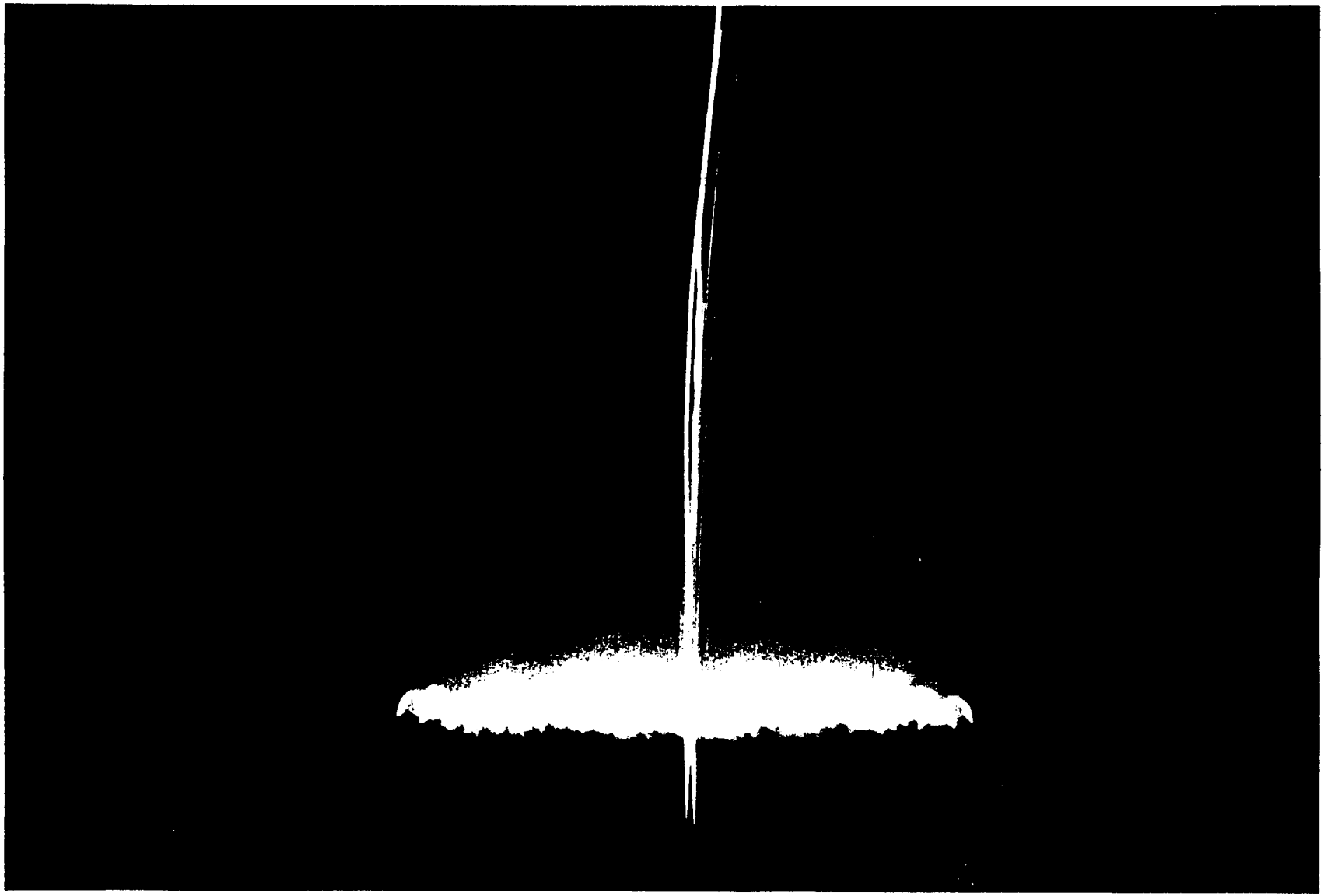

Figure 25: Sun Slurry Combustion at an Equivalence Ratio of 0.5 and an Oxidant O_2 Mass Fraction of 0.25 Showing Both RP-1 and Aluminum Combustion.

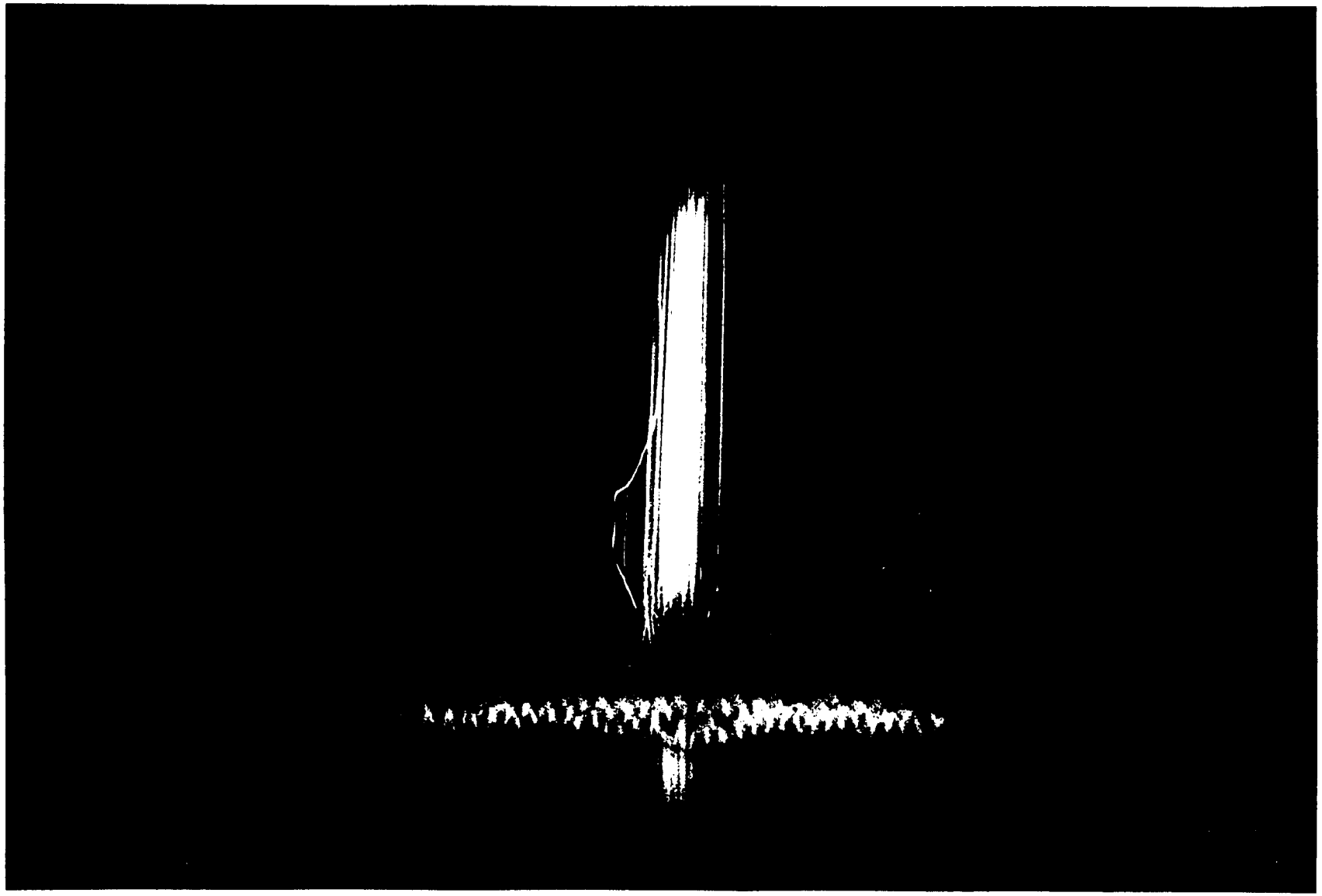

Figure 26: Sun Slurry Combustion at an Equivalence Ratio of 0.5 and an Oxidant O_2 Mass Fraction of 0.25 Showing a Particle Undergoing Micro-Fragmentation.

FUTURE PLANS

During the next 6-month period the following activities are planned:

1. Measure the optical pinholes using a scanning electron microscope.

2. Complete electronics shakedown.

3. Continued shakedown of the data acquisition and analysis system using the vibrating orifice droplet generator, pure liquids and aluminum slurry fuels.

4. Integrated operation of the complete system (burner, spray rig, particle sizing and velocimetry system, data acquisition, and data processing) using aluminum slurry fuels.

5. Shakedown ignition detection system.

6. Begin parametric study using baseline slurry.

7. Modify existing ignition codes.

8. Preliminary formulation of disruptive ignition model.

9. Measure temperature field in product gases.

REFERENCES

1. Wang, J. C. F., and Hencken, K. R., "In Situ Particle Size Measurements Using a Two-Color Laser Scattering Technique," Applied Optics, 25:653-657, 1986.

2. Kent, J. H., "A Non-Catalytic Coating for Platinum-Rhodium Thermocouples," Combustion and Flame, 14:279-281, 1970.